Inorganic Chemistry

Article

pubs.acs.org/IC

Revealing Disparate Chemistries of Protactinium and Uranium. Synthesis of the Molecular Uranium Tetroxide Anion, UO_4^-

Wibe A. de Jong,*[,†] Phuong D. Dau,[‡] Richard E. Wilson,[§] Joaquim Marçalo,[∥] Michael J. Van Stipdonk,[⊥] Theodore A. Corcovilos,[#] Giel Berden,[7] Jonathan Martens,[7] Jos Oomens,[7,8] and John K. Gibson*[,‡]

[†]Computational Research Division, Lawrence Berkeley National Laboratory, Berkeley, California 94720, United States

[‡]Chemical Sciences Division, Lawrence Berkeley National Laboratory, Berkeley, California 94720, United States

[§]Chemical Sciences and Engineering Division, Argonne National Laboratory, Argonne, Illinois 60439, United States

[∥]Centro de Ciências e Tecnologias Nucleares, Instituto Superior Técnico, Universidade de Lisboa, 2695-066 Bobadela Loures, Portugal

[⊥]Department of Chemistry and Biochemistry, Duquesne University, Pittsburgh, Pennsylvania 15282, United States

[#]Department of Physics, Duquesne University, Pittsburgh, Pennsylvania 15282, United States

[7]Radboud University, Institute for Molecules and Materials, FELIX Laboratory, Toernooiveld 7c, 6525ED Nijmegen, The Netherlands

[8]van 't Hoff Institute for Molecular Sciences, University of Amsterdam, Science Park 904, 1098XH Amsterdam, The Netherlands

Supporting Information

ABSTRACT: The synthesis, reactivity, structures, and bonding in gas-phase binary and complex oxide anion molecules of protactinium and uranium have been studied by experiment and theory. The oxalate ions, $An^{V}O_2(C_2O_4)^-$, where An = Pa or U, are essentially actinyl ions, $An^{V}O_2^+$, coordinated by an oxalate dianion. Both react with water to yield the pentavalent hydroxides, $An^{V}O(OH)_2(C_2O_4)^-$. The chemistry of Pa and U becomes divergent for reactions that result in oxidation: whereas Pa^{VI} is inaccessible, U^{VI} is very stable. The $U^{V}O_2(C_2O_4)^-$ complex exhibits a remarkable spontaneous exothermic replacement of the oxalate ligand by O_2 to yield UO_4^- and two CO_2 molecules. The structure of the uranium tetroxide anion is computed to correspond to distorted uranyl, $U^{VI}O_2^{2+}$, coordinated in the equatorial plane by two equivalent O atoms each having *formal* charges of −1.5 and U−O bond orders intermediate between single and double. The unreactive nature of $Pa^{V}O_2(C_2O_4)^-$ toward O_2 is a manifestation of the resistance toward oxidation of Pa^{V}, and clearly reveals the disparate chemistries of Pa and U. The uranium tetroxide anion, UO_4^-, reacts with water to yield $UO_5H_2^-$. Infrared spectra obtained for $UO_5H_2^-$ confirm the computed lowest-energy structure, $UO_3(OH)_2^-$.

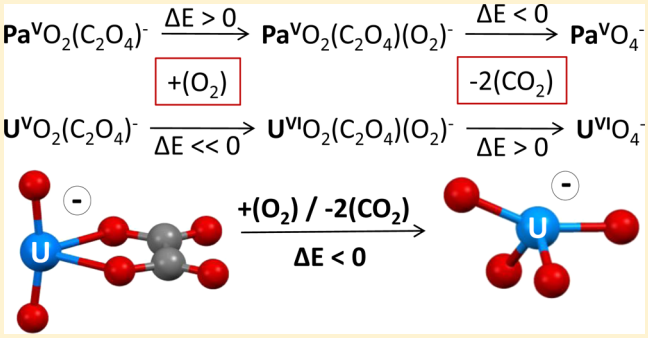

INTRODUCTION

Gas-phase chemistry has been demonstrated as an effective approach for revealing new and fundamental aspects of metal ion chemistry.[1−10] An attribute of these systems is that they are generally sufficiently simple that accurate computational modeling is feasible, even for systems that incorporate many-electron heavy elements such as actinides.[11] Bonding and reactivity of gas-phase actinide oxides, particularly uranium oxides, has received appreciable attention, both experimentally and computationally.[12−25] Of particular interest are molecules with an excess of oxygen atoms, such as UO_4^-, in which not all can be accommodated as O^{2-} moieties within the constraint of the highest accessible hexavalent oxidation state of uranium. In such cases the excess O atoms are accommodated either as open-shell oxo-ligands with radical character, or as ligands with O−O bonding. In most reported uranium oxide molecules the (nearly) linear uranyl moiety with two strongly bound O atoms is retained, and the excess O atoms adopt alternative bonding configurations.[17,26,27]

Whereas uranium oxides have received considerable attention, oxides of the much less prevalent and more radioactive actinide protactinium have been relatively neglected. Preceding U in the actinide series, Pa has one less valence electron and thus typically exhibits Pa^{V} as its highest oxidation state. Because of this fundamental difference in the chemistries of Pa and U, it is expected that there should not necessarily be a correspondence between these two elements upon addition of

Received: January 17, 2017
Published: March 9, 2017

DOI: 10.1021/acs.inorgchem.7b00144
Inorg. Chem. 2017, 56, 3686−3694

O atoms beyond the pentavalent anion oxides, $An^{V}O_3^-$. Already for pentavalent ions the chemistry between Pa and U is different. $Pa^{V}O_2^+$ rapidly hydrolyzes in aqueous solution, this in contrast to hydration of $U^{V}O_2^+$,[28−30] a difference that has also been observed in the gas phase.[31] Reactions of neutral or charged Pa^{V} and U^{V} oxide molecules should reveal fundamental differences in chemistry, particularly regarding oxygen-rich species where the excess O atoms can be accommodated in different manners. In addition to binary oxides, more complex species comprising Pa^{V} and $U^{V/VI}$ with actinyl cores coordinated by anionic ligands can provide insights into variations in chemistry between these two neighboring actinides.

Previous chemistry and spectroscopy studies of gas-phase uranium oxide anions, including UO_4^-, have relied on high-energy synthesis methods such as laser ablation of solids or energetic fragmentation of gas-phase precursor complexes that have been produced under low-energy conditions such as by electrospray ionization (ESI) of complexes in solution.[17,27,32] A goal of gas-phase chemistry is to identify spontaneous exothermic reactions that can alternatively result in seemingly exotic high-energy species such as UO_4^- under thermal conditions. One approach to achieve such reactions is by selecting precursors that have ligands that decompose absent substantial kinetic barriers to yield stable neutral molecules, such as CO_2.

The overall objective of the present work was to explore the chemistries of gas-phase binary and complex protactinium and uranium oxide species. An emphasis was on differences between these two neighboring actinides, which contrasts with the very similar chemistries of the homologous trivalent 4f lanthanides, Pr and Nd. A further aim was to identify a route to oxygen-rich molecular ions via ion−molecule reactions under thermal conditions; a new synthetic route to molecular UO_4^- was identified. The gas-phase pentavalent actinyl complexes $PaO_2(C_2O_4)^-$ and $UO_2(C_2O_4)^-$ were produced by very different approaches, a disparity that reflects very different chemistries of Pa^{V} and U^{V}. Gas-phase reactions of the two pentavalent actinyl-oxalate complexes with H_2O and O_2 were studied in a quadrupole ion trap (QIT), with contrasting results that reveal different chemistries of Pa and U. Infrared multiphoton dissociation (IRMPD) spectra were acquired for selected gas-phase uranium complexes. The structures and bonding of the oxalate complexes and reaction products were computed using density functional theory (DFT); agreement between experiment and theory provides validation of the computational methodology, as well as of computational results not directly evaluated by experimental results.

EXPERIMENTAL APPROACH

The general experimental approach has been described previously.[33] The anionic actinyl carboxylate complex, $UO_2(C_2O_4)^-$, was produced by ESI of an ethanol solution prepared by diluting a 10 mM UO_2Cl_2 stock solution (^{238}U isotope; pH = 2) to 100 μM; $H_2C_2O_4$ was added to yield a $H_2C_2O_4$:U ratio of 3:1. A 14 mM solution of Pa in 0.1 M HCl, containing a 6:1 ratio of NH_4F:Pa so as to solubilize the $Pa_2O_5\cdot xH_2O$ was used as a stock solution. This Pa stock was diluted with 1 M $H_2C_2O_4$ corresponding to a $H_2C_2O_4$:F^- ratio of 500:1, in an effort to displace the strongly coordinating F^- from the Pa. Prior to addition of excess oxalate, PaF_6^- was evident in the ESI mass spectrum. The Pa oxalate solution was introduced to the mass spectrometer as a 50% vol/vol ethanol to $Pa_{(aq)}$ mixture, resulting in a final $H_2C_2O_4$:Pa ratio of 3500:1. As discussed below, ESI of the Pa solution did not directly yield $PaO_2(C_2O_4)^-$, which was instead prepared by fragmentation of gas-phase $Pa(C_2O_4)_3^-$.

Caution! *The employed ^{231}Pa isotope is highly radioactive with an α-decay half-life of ∼33000 y; the radiological hazards are highly exacerbated by the several short-lived progeny in the subsequent decay chain, starting with daughter ^{227}Ac. Accordingly, ^{231}Pa must be handled with proper radiological safety controls.*[34]

The experiments were performed using an Agilent 6340 ESI QIT mass spectrometer (QIT/MS) with MS^n collision induced dissociation (CID) capability; the CID energy is an instrumental parameter that provides an indication of relative ion excitation.

Mass-selected ions in the trap can undergo ion−molecule reactions at ∼300 K[35] by applying a reaction time of up to 10 s. Anion mass spectra were acquired using the following parameters: solution flow rate, 60 μL/h; nebulizer gas pressure, 12 psi; capillary voltage offset and current, −4000 V and 210 nA; end plate voltage offset and current, −500 V and 3000 nA ; dry gas flow rate, 3 l/min; dry gas temperature, 325 °C; capillary exit, −50.0 V; skimmer, −36 V; octopole 1 and 2 DC, −10.9 V and −3.0 V; octopole RF amplitude, 190 Vpp; lens 1 and 2, 10.0, and 91.0 V; trap drive, 50.0. Nitrogen gas for nebulization and drying was supplied from the boil-off of a liquid nitrogen Dewar. The background water and oxygen pressures in the ion trap are estimated as $\sim10^{-6}$ Torr. Reproducibility of hydration rates of $UO_2(OH)^+$ established that the water pressure was constant to within ∼10%;[36] reproducibility of O_2-addition to $UO_2(CH_3COO)_2^-$ established a similar constancy of the oxygen pressure.[37] The helium buffer gas pressure in the trap is constant at $\sim10^{-4}$ Torr.

The ion trap has been modified to allow for the introduction of reagent gases through a gas manifold and a leak valve.[34] The $^{18}O_2$ gas was directly introduced into the ion trap. Although the isotopic purity of the $^{18}O_2$ was unknown, the relative pressure of $^{18}O_2$ and $^{16}O_2$ was determined by monitoring the previously reported reaction of $UO_2(CH_3CO_2)_2^-$ with O_2 to yield $UO_2(O_2)(CH_3CO_2)_2^-$.[37]

The IRMPD experiments were performed at the Free Electron Laser for Infrared Experiments (FELIX) Laboratory.[38] The $UO_2(C_2O_4)^-$ complex was produced by ESI of a similar solution and under similar conditions as employed for the gas-phase reactivity studies described above; the $UO_3H_2^-$ complex resulted from the sequential reaction of $UO_2(C_2O_4)^-$ with O_2 and H_2O as described below. The IRMPD spectra were acquired using a QIT/MS similar to that previously employed to study uranyl-crown and organouranyl complexes.[39,40] The QIT/MS has been modified[41,42] such that the high-intensity tunable IR beam from FELIX can be directed onto the ion packet, resulting in multiphoton dissociation that is appreciable only when the IR frequency is resonant with a sufficiently intense absorption vibrational mode of the particular mass-selected complex being studied. The FEL produces ∼5 μs long IR pulses with an energy of ∼40 mJ/pulse at a repetition rate of 10 Hz. For the IRMPD measurements described here, ions were irradiated for 200 ms, corresponding to two FEL pulses, before being scanned out of the trap and detected.

COMPUTATIONAL METHODS

All the calculations in the manuscript were performed with the latest development version of the open-source NWChem software suite.[43] Density functional theory calculations were carried out with the PBE0[44] density functional, using the Stuttgart small-core effective core-potential for the actinide atoms[45] and all-electron DFT optimized valence triple-ζ polarized (TZVP) basis sets[46] for the light atoms in the complex. An unrestricted wave function was used for all open-shell DFT calculations. The geometries of the complexes were optimized, followed by frequency calculations to ensure the calculated structure had no imaginary frequencies and was in a minimum energy configuration. All calculated energetics presented in this paper include the zero-point energy correction. For each experimentally observed species all possible bonding and coordination patterns were explored at various accessible spin states. Oxidation states were assigned based on Mulliken atomic spin populations. Atomic spin populations have been shown to provide a reliable picture of the actinide oxidation state

DOI: 10.1021/acs.inorgchem.7b00144
Inorg. Chem. 2017, 56, 3686−3694

Table 1. Computed Reaction Energies[a]

	reaction	An = Pa	An = U
1	$An(C_2O_4)_3^- \rightarrow AnO(C_2O_4)_2^- + CO_2 + CO$	206	
2	$AnO(C_2O_4)_2^- \rightarrow AnO_2(C_2O_4)^- + CO_2 + CO$	189	
3	$AnO_2(C_2O_4)^- + H_2O \rightarrow AnO_2(C_2O_4)(H_2O)^-$	−73	−75
4	$AnO_2(C_2O_4)^- + H_2O \rightarrow AnO(OH)_2(C_2O_4)^-$	−121	−95
5	$AnO(C_2O_4)_2^- + H_2O \rightarrow AnO(C_2O_4)_2(H_2O)^-$	−79	
6	$AnO(C_2O_4)_2^- + H_2O \rightarrow An(OH)_2(C_2O_4)_2^-$	−132	
7	$AnO_2(C_2O_4)^- + O_2 \rightarrow AnO_2(C_2O_4)(O_2)^-$	52	−218
8	$AnO_2(C_2O_4)(O_2)^- \rightarrow AnO_4^- + 2(CO_2)$	−45	78
9	$AnO_2(C_2O_4)^- + O_2 \rightarrow AnO_4^- + 2(CO_2)$	7	−140
11	$AnO_4^- + H_2O \rightarrow AnO_4(H_2O)^-$	−9	−57
12	$AnO_4^- + H_2O \rightarrow AnO_3(OH)_2^-$	−187	−171

[a]ΔE in kJ/mol, with zero point energy correction.

by Maurice et al.[47] A QTAIM analysis of the bond critical points in the actinyls was performed with the AIMAll code.[48]

RESULTS AND DISCUSSION

Synthesis and Structures of $AnO_2(C_2O_4)^-$ (An = Pa, U). The complex $UO_2(C_2O_4)^-$ was produced directly by ESI of a solution containing uranyl and oxalic acid (Figure S2). Formation of the $U^VO_2^+$ oxalate complex indicates reduction of $U^{VI}O_2^{2+}$ during ESI. Also apparent in the ESI mass spectrum is a peak attributed to the $U^{VI}O_2^{2+}$ oxalate dianion complex, $UO_2(C_2O_4)_2^{2-}$, which upon CID yields $UO_2(C_2O_4)^-$ and $C_2O_4^-$ (the latter ion is not detected due to the low-mass cutoff of the QIT/MS during CID). In contrast to uranyl, protactinyl is not a stable species in solution but rather undergoes hydrolysis.[28,29] Accordingly, $PaO_2(C_2O_4)^-$ did not appear in the ESI mass spectrum. Instead, the gas-phase protactinyl complex was produced by CID of the Pa^V complex, $Pa(C_2O_4)_3^-$, which was a prominent species in the ESI mass spectrum (Figure S1). Primary CID (MS^2) of $Pa(C_2O_4)_3^-$ yields predominantly $PaO(C_2O_4)_2^-$. Secondary CID of $PaO(C_2O_4)_2^-$ (MS^3) yields $PaO_2(C_2O_4)^-$, along with substantial $PaO(OH)_2(C_2O_4)^-$, which is attributed to a hydrolysis reaction with background water in the ion trap (see below). The syntheses of the protactinyl oxalate complex was achieved by CID reactions 1 and 2 in Table 1, which are facilitated by the formation of the stable CO_2 and CO molecules.

The computed ground state structures of $UO_2(C_2O_4)^-$ and $PaO_2(C_2O_4)^-$ are shown in Figure 1. The O−An−O actinyl

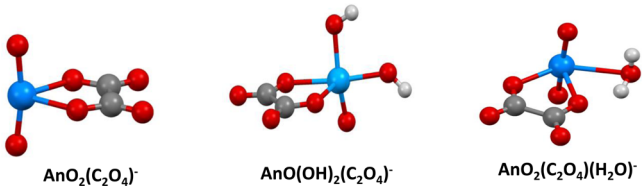

Figure 1. Computed structures of $AnO_2(C_2O_4)^-$, $AnO(OH)_2(C_2O_4)^-$, and $AnO_2(C_2O_4)(H_2O)^-$ for An = Pa and U.

bond angles are 154.2° and 165.0°, and the An−O_{yl} bond distances are 1.87 and 1.81 Å for An = Pa and U, respectively (all geometric coordinates are in the Supporting Information). Both actinyls are distorted from linear, with that for protactinyl substantially more so. Although the net bond dissociation energy, to An^+ and two O atoms, of PaO_2^+ (~1580 kJ/mol) is somewhat greater than that of UO_2^+ (~1520 kJ/mol), it has been established that molecular Pa−O bonds are less covalent than U−O bonds due to energy-degeneracy driven covalency.[31,49,50] A QTAIM analysis of two of the bond critical point (BCP) metrics along the An-O bond, namely the electron (Pa = 0.237 au, U = 0.275 au) and energy (Pa = −0.168 au, U = −0.229 au), show an increase in value that is indicative of an increased covalency going from Pa to U.[50] The greater deviation from linearity for protactinyl can be attributed to this lesser covalency, which relaxes the necessity for symmetry correspondence between the Pa 5f and O 2p orbitals. The greater propensity for PaO_2^+, when compared with other pentavalent actinyl ions, to hydrolyze has similarly been attributed to its more ionic bonding character.[51] The results of the bonding analysis for $UO_2(C_2O_4)^-$ and $PaO_2(C_2O_4)^-$ in Table 2 indicate spin populations and states, and atomic charges, in accord with characterization of these as pentavalent actinyl complexes. The parameters in Table 2 are indicative of pentavalent actinyl complexes that are formally $Pa(5f^0)O_2^+$ and $U(5f^1)O_2^+$ coordinated by an oxalate dianion, $C_2O_4^{2-}$. The $PaO_2(C_2O_4)^-$ complex synthesized in this work is a rare example of a $Pa^VO_2^+$ species, which are virtually unknown due to the propensity of protactinyl to hydrolyze.[52] This accomplishment is an illustration of the ability to produce stable prototypical bonding motifs that may be inaccessible in the condensed phase due to high reactivity; the proclivity for $PaO_2(C_2O_4)^-$ to hydrolyze during CID is in correspondence with the intrinsic solution chemistry of Pa^V.

Addition of H_2O to $AnO_2(C_2O_4)^-$ and $PaO(C_2O_4)^-$. Experimental results for reactions of $PaO_2(C_2O_4)^-$ and $UO_2(C_2O_4)^-$ with background gases in the ion trap are shown in Figure 2. As has been discussed previously,[36,37] the background pressures of H_2O and O_2 in the QIT are estimated to be on the order of ~10^{-6} Torr, and are found to remain constant to within ~10%. For the Pa complex the only observed reaction is water-addition, which is also observed for the U complex albeit with an efficiency more than ten times lower and with additional reaction pathways as discussed below. Water-addition can result in a hydrate by simple adduct formation (reaction 3 in Table 1), or a bis-hydroxide by hydrolysis (reaction 4 in Table 1). The computed structures for both the hydroxide and hydrate isomers, which are similar for An = Pa and U, are shown in Figure 1. The computed energetics for hydrate and hydroxide formation are given in Table 1 (reactions 3 and 4, respectively), where it is apparent that the hydroxide is predicted to be the more stable isomer upon addition of a water molecule to both the Pa and U complexes. Whereas the physisorption hydration reactions exhibit very similar energies for both complexes, the

DOI: 10.1021/acs.inorgchem.7b00144
Inorg. Chem. 2017, 56, 3686−3694

Table 2. Spin States, Mulliken Atomic Charges (q), Atomic Spin Populations (μ) of Actinyl Oxygens, and Assigned Oxidation States for $PaO_2(C_2O_4)^-$, $UO_2(C_2O_4)^-$, $PaO_2(C_2O_4)(O_2)^-$, $UO_2(C_2O_4)(O_2)^-$, PaO_4^-, and UO_4^-

species	An	q_{An}	μ_{An}	$q_{O\text{-}AnO_2}$	$\mu_{O\text{-}AnO_2}$	q_{O-O_2}	μ_{O-O_2}	oxidation/spin state
$AnO_2(C_2O_4)^-$	Pa	1.67	0.00	−0.69	0.00			V ($5f^0$)/singlet
	U	1.60	1.12	−0.67	−0.05			V ($5f^1$)/doublet
$AnO_2(C_2O_4)(O_2)^-$	Pa	1.78	0.24	−0.59	0.30	−0.23	0.51	V ($5f^0$)/triplet[a]
	U	1.75	−0.05	−0.57	0.00	−0.21	0.52	VI ($5f^0$)/doublet
AnO_4^-	Pa	1.56	0.00	−0.77/−0.51	0.00/0.00			V ($5f^0$)/singlet
	U	1.70	−0.20	−0.66/−0.69	0.19/0.41			VI ($5f^0$)/doublet

[a]Triplet is energetically degenerate with the open-shell singlet.

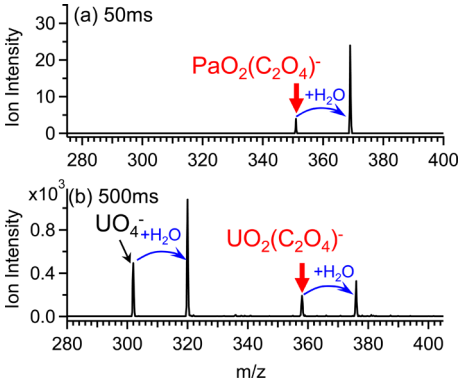

Figure 2. Mass spectra acquired after isolation of (a) $PaO_2(C_2O_4)^-$ and (b) $UO_2(C_2O_4)^-$ and reaction with background gases (H_2O and O_2) in the ion trap for 50 and 500 ms, respectively. The black arrow points to the UO_4^-, whereas the red arrows point to $PaO_2(C_2O_4)^-$ in panel a and $UO_2(C_2O_4)^-$ in panel b. Blue arrows signify water addition products.

chemisorption hydrolysis reaction is calculated to be 26 kJ/mol more exothermic for $PaO_2(C_2O_4)^-$ versus $UO_2(C_2O_4)^-$, which could account for the faster reaction rate for the Pa complex. The greater propensity for hydrolysis of the protactinyl complex is in accord with previous results for water-addition to PaO_2^+ versus UO_2^+, where the former hydrolyzes to a bis-hydroxide whereas the latter forms a hydrate adduct. This disparity in chemistry may be ascribed to lesser covalency of molecular Pa−O bonds, as discussed previously.[31,49,50] Addition of water to the $AnO_2(C_2O_4)^-$ complexes, whether the product is a bis-hydroxide or a hydrate, results in no change in oxidation state with the result that the energetics for the Pa and U complexes are similar. This is in contrast to reactions for which there is a change in oxidation state, specifically from U^V to U^{VI} as occurs in the addition of O_2 to yield a superoxide; for this oxidation reaction the energetics are significantly more favorable for U^V versus Pa^V because of the stability of the U^{VI} oxidation state.

The computed energetics for the hydrate and hydroxide formation for $PaO(C_2O_4)_2^-$ (reactions 5 and 6) and $PaO_2(C_2O_4)^-$ (reactions 3 and 4) are found to be very similar. Because primary and sequential CID of $Pa(C_2O_4)_3^-$ yielded both $PaO(C_2O_4)_2^-$ and $PaO_2(C_2O_4)^-$ it was possible to directly compare the hydrolysis rates of these two anion oxo complexes. The results (Figure S3) reveal that $PaO_2(C_2O_4)^-$ hydrolyzes much more rapidly, by a factor of ∼100-fold, as compared with $PaO(C_2O_4)_2^-$. Given the reaction energetics were found to be similar, the difference in reactivity is driven by a higher kinetic barrier for $PaO(C_2O_4)_2^-$. The two species can be considered as PaO_2^+ and PaO^{3+} coordinated by one or two oxalate dianions, respectively. It is known that PaO_2^+ is highly susceptible to hydrolysis in aqueous solution, whereas PaO^{3+} exhibits a substantially greater stability.[53] The gas-phase hydrolysis results are found to be parallel to the solution hydrolysis behavior of PaO_2^+ and PaO^{3+}, where the former is more susceptible toward hydrolysis. In particular, the much more facile hydrolysis of the PaO_2^+ core to yield $PaO(OH)_2(C_2O_4)^-$ is in accord with the unstable nature of this dioxo cation. This chemistry is not fully understood but is generally attributed to highly ionic character of the Pa−O bonds in PaO_2^+, which results in more facile attack by water to yield Pa−OH bonds upon hydrolysis.[31,49−51]

Reactions of $AnO_2(C_2O_4)^-$ with O_2: The Synthesis of UO_4^-. A particularly notable result is the appearance of UO_4^- upon reaction of $UO_2(C_2O_4)^-$ with background gases in the ion trap (Figure 2b). The corresponding PaO_4^- product is not apparent in Figure 2a. To confirm that UO_4^- results from the reaction of $UO_2(C_2O_4)^-$ with O_2, an excess of isotopically labeled $^{18}O_2$ was introduced into the ion trap. The result is shown in Figure 3, where the dominant product peak at 306 m/z corresponds to reaction of $UO_2(C_2O_4)^-$ with $^{18}O_2$ to yield $UO_2{}^{18}O_2$ (unless specified otherwise, O refers to the 99.8% natural abundance ^{16}O isotope). The minor peak at 304 m/z is attributed to oxo-exchange of $UO_2{}^{18}O_2^-$ with background water in the trap to yield $UO_3{}^{18}O^-$. That this exchange process occurs was established by demonstrating exchange of UO_4^- with $H_2{}^{18}O$ (Figure S4). The minor peak at 302 m/z corresponds to reaction of $UO_2(C_2O_4)^-$ with background O_2 in the trap to yield UO_4^-, as is apparent in Figure 2b. There is also a minor peak at 376 m/z resulting from addition of H_2O to $UO_2(C_2O_4)^-$; the intensity of this peak is much lower than in Figure 2b, largely due to the shorter reaction time, 50 ms there versus 500 ms in Figure 3.

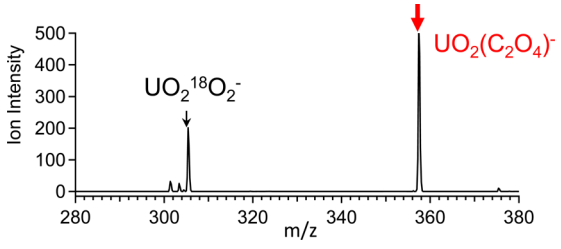

Figure 3. Mass spectrum acquired after isolation of $UO_2(C_2O_4)^-$ for 50 ms in the ion trap containing $^{18}O_2$. The $^{16}O_2/^{18}O_2$ ratio was estimated as ∼1:8 using the method described in the Experimental Section.

Spontaneous exothermic replacement of C_2O_4 by O_2 in $UO_2(C_2O_4)^-$ to yield UO_4^- is a remarkable process. Notably, this replacement reaction is not observed for $PaO_2(C_2O_4)^-$. The observed reaction presumably occurs by addition of O_2 to

DOI: 10.1021/acs.inorgchem.7b00144
Inorg. Chem. 2017, 56, 3686−3694

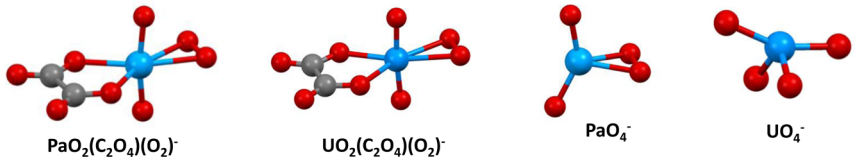

Figure 4. Computed structures of $AnO_2(C_2O_4)(O_2)^-$ and AnO_4^- for An = Pa, U.

the oxalate complex, reaction 7 in Table 1, followed by elimination of two CO_2 molecules, reaction 8. The weakly bound C_2O_4 gas-phase CO_2 dimer complex is calculated to be a few kJ/mol lower in energy than two separated CO_2 molecules and should not remain bound under the ~300 K experimental conditions; the product of reaction 8 is accordingly given as two CO_2 molecules rather than the dimer. The computed energies for the O_2-addition reaction 7, CO_2-elimination reaction 8, and the net O_2/C_2O_4 replacement reaction 9 are given in Table 1. For protactinium the O_2 association reaction is unfavorable, and as a result the replacement reaction is not observed in experiment. In contrast, the O_2 association with the uranium complex is highly exothermic. In the formation of $UO_2(C_2O_4)(O_2)^-$ the uranium gets oxidized to U^{VI}. Protactium cannot be oxidized further, and forms an unstable biradical complex where the triplet and open-shell singlet are nearly degenerate, with one unpaired electron on the O_2 and one electron distributed over the PaO_2 unit. The experimental result that the association complex $UO_2(C_2O_4)(O_2)^-$ is not observed suggests that it efficiently eliminates two CO_2 molecules to yield UO_4^- according to reaction 9 in Table 1.

Reaction 10, in which $U^VO_2^+$ anion complexes are oxidized to $U^{VI}O_2^{2+}$ by addition of O_2 to form superoxides, was previously reported to occur spontaneously for X = F, Cl, Br, I, OH, NO_3, ClO_4, HCO_2, CH_3CO_2, CF_3CO_2, CH_3COS, NCS, and N_3.[37]

$$U^VO_2X_2^- + O_2 \rightarrow U^{VI}O_2X_2(O_2)^- \quad (10)$$

The energy for reaction 10 was computed for X = F, Cl, Br, I, OH, and NCS; the results indicated the reaction to be exothermic by 143 kJ/mol (for X = I) to 195 kJ/mol (for X = OH). The computed energy of reaction 7 for An = U is only 23 kJ/mol more exothermic than is reaction 10 for X = OH. Some care should be taken comparing the energetics as the density functional used here differs from the previous work. Even so, it is apparent that reaction 7 for An = U is directly analogous to reaction 10, with two X^- ligands replaced by one $C_2O_4^{2-}$ ligand.

The computed structures and properties of $UO_2(C_2O_4)(O_2)^-$ are consistent with the characterization as a U^{VI} superoxide complex (Figure 4 and SI). The $U^VO_2X_2^-$ and $U^VO_2(C_2O_4)^-$ complexes are exothermically oxidized to $U^{VI}O_2^{2+}$ by addition of O_2 to yield superoxides. For the $U^{VI}O_2X_2(O_2)^-$ products there is no low-energy dissociation pathway and a substantial fraction of the adduct cools by collisions with the helium bath gas in the ion trap and thus remains intact prior to adiabatic dissociation to the reactants. For the $UO_2(C_2O_4)(O_2)^-$ association product, the energy for the pathway corresponding to elimination of two CO_2 molecules is much lower than the association energy and is thus enabled after association. Notably, $UO_2(C_2O_4)(O_2)^-$ was not detected—there is no peak at 390 *m/z* in Figure 2b—suggesting that carbon dioxide elimination predominates during the period before the association complex has cooled to an energy below the 78 kJ/mol needed for this process. The proposed reaction pathways and energetics are shown in Figure 5.

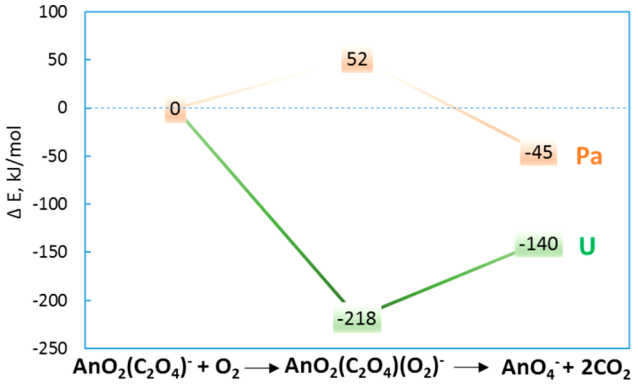

Figure 5. Computed reaction energetics for conversion of $AnO_2(C_2O_4)^-$ to AnO_4^- by reaction with O_2. Although the overall reaction is predicted to be exothermic for An = Pa and U, the initial O_2-assciation step is endothermic for Pa but exothermic for U.

As is apparent in Figure 2, the only reaction of $PaO_2(C_2O_4)^-$ with the H_2O/O_2 background gases in the ion trap is water addition, which results in no change in oxidation state. Oxidation of closed-shell $[Rn]5f^0$ Pa^V is chemically implausible with the result that addition of O_2 to yield the superoxide $PaO_2(C_2O_4)(O_2)^-$ is not favorable. The calculated energetics show that reaction 7 is endothermic by 52 kJ/mol for Pa, and is 270 kJ/mol less favorable than for U. This is a manifestation of relatively facile oxidation of U^V to U^{VI}, this in contrast to the inaccessibility of the Pa^{VI} oxidation state. As indicated in Table 2, the oxidation state of the hypothetical $PaO_2(C_2O_4)(O_2)^-$ is predicted to stay Pa^V. This complex is also computationally shown to be unstable relative to PaO_4^- and two CO_2 molecules (reaction 9 in Table 1).

The computed structures of hypothetical PaO_4^- and observed UO_4^- are shown in Figure 4, with all of the structural parameters included in the Supporting Information. The structure of PaO_4^- incorporates a distorted protactinyl moiety in which the O_{ax}–Pa–O_{ax} angle is 144° and the Pa–O_{ax} bond distances are both 1.91 Å. The formally PaO_2^+ unit is coordinated by a peroxide ligand to yield the $Pa^VO_4^-$ anion complex with Pa–O_{per} distances of 2.19 Å and an O_{per}–O_{per} distance of 1.46 Å. The distinctive UO_4^- complex, where the O_2 is clearly dissociated (bond distance of over 3 Å), is computed to have a $5f^0$ configuration corresponding to U^{VI}. The symmetry of the species is C_{2v}: there are two uranyl double bonds with U–O distances of 1.84 Å and an O_{ax}–U–O_{ax} angle of 157°, and two longer and weaker bonds having U–O distances of 1.92 Å and an O_{ax}–U-O_{ax} angle of 114°. The atomic properties are in Table 2. Alternative structures were found to be higher in energy, for example the $U^VO_2^+$-peroxo was calculated to be 130 kJ/mol higher in energy. The

DOI: 10.1021/acs.inorgchem.7b00144
Inorg. Chem. 2017, 56, 3686–3694

computed structure of UO_4^- is very similar to that reported and analyzed previously.[17,54] The doublet spin state indicates one unpaired electron distributed between the two more weakly bonded oxygen atoms. This interpretation is very similar to that of Michelini and co-workers, who find the radical character to be delocalized between the same "equatorial" oxygen atoms.[17] More recently Su et al.[54] studied the unusual structure of UO_4^- and came to a consistent conclusion that the complex is not fully represented with fractional oxidation states $2O_{ax}^{2-}$ and $2O^{-1.5}$, as suggested here, but is rather intermediate between this and four $O^{-1.75}$ ligands as would be the case if all U−O bonds would be equal. Although the bonding representation presented here is a somewhat simplified model, it conveys the essential nature of the species.

Reaction of UO_4^- with H_2O. The addition of water to UO_4^- is apparent in Figure 2b. It is conceivable from these results that $UO_5H_2^-$ is produced from a secondary reaction of $UO_2(OH)_2(C_2O_4)^-$. To confirm direct water addition to the tetroxide, UO_4^- was isolated and reacted with the background gases. The result is shown in Figure 6, where it is apparent that

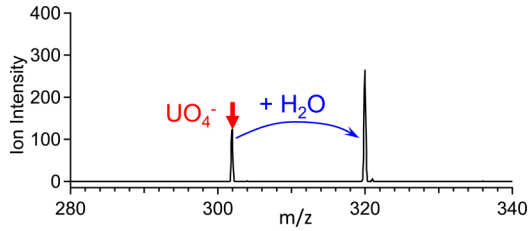

Figure 6. Mass spectrum acquired after isolation of UO_4^- for 300 ms in the ion trap containing background gases. The result demonstrates the spontaneous addition of H_2O to UO_4^-.

water addition to UO_4^- occurs spontaneously. As is the case for water addition to the oxalates, the two plausible structures for the water-addition product are a hydrate, $UO_4(H_2O)^-$, and a hydroxide, $UO_3(OH)_2^-$. The calculated energies for the two water-addition processes, reactions 11 and 12, are given in Table 1 for both hypothetical PaO_4^- and observed UO_4^-. In both cases the formation of the hydroxide, reaction 12, is calculated to be substantially more energetically favorable than formation of the hydrate; the energy disparities between physisorption and chemisorption are greater than for water addition to the oxalates as given by reactions 3 and 4 (Table 1). The formation of hydroxide rather than hydrate motif upon reaction of gaseous metal oxo complexes with water is not unprecedented.[55] The computed structures of all of the water-addition species are included in the Supporting Information. The structure of ground-state doublet $UO_3(OH)_2^-$ is nearly linear uranyl ($\angle O_{ax}$−U-O_{ax} = 177°) with three ligands, two OH and one O, in the equatorial plane, separated by angles close to 120°. The U−O_{ax} distances of 1.79 Å are typical of uranyl bonds. The U−OH distances of 2.20 Å are characteristic of U−O single bonds. The U−O_{eq} distance, 2.18 Å, is similarly indicative of a single bond such that the complex can be considered as $U^{VI}O_2^{2+}$ coordinated by two hydroxide ligands and a radical oxygen atom with an unpaired electron. The computed structure of ground-state singlet $PaO_3(OH)_2^-$ is very different: Pa is coordinated by a double-bond oxygen, two hydroxides, and a peroxide moiety to yield the stable pentavalent oxidation state.

IRMPD Spectrum of $UO_5H_2^-$. IRMPD spectra were acquired in an ion trap at FELIX that has a similar design to that employed for the CID and reactivity studies at LBNL. The time scale of the IRMPD experiments—ion accumulation and IRMPD dissociation—is ~200 ms, which is shorter but roughly comparable to the 500 ms time scale of the reactivity results shown in Figure 2b. As is apparent in Figures 2 and 6, the product resulting from addition of H_2O to UO_4^- is unreactive on this same time scale under the experimental conditions. It was thus possible to acquire an IRMPD spectrum for this species. The spectrum, shown in Figure 7, was obtained by isolating UO_4^- (302 *m*/*z*), after which the $UO_5H_2^-$ water-addition product was also present in the ion trap; both of these species were present during the IRMPD experiment. Upon varying the FEL wavelength it was observed that depletion of $UO_5H_2^-$ resulted in enhancement of the IRMPD product ion UO_4^-. The IRMPD spectrum was thus acquired by measuring the increase in UO_4^- above the baseline intensity as the wavelength was varied. The resulting spectrum acquired in the

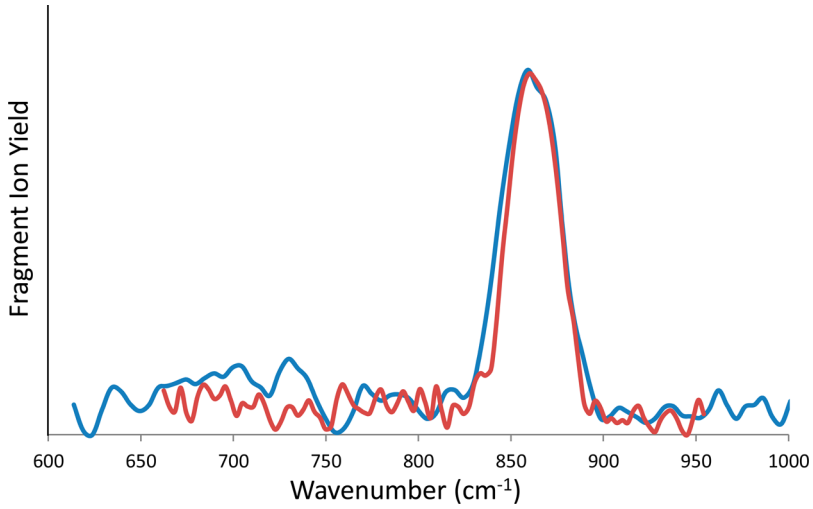

Figure 7. Two IRMPD spectra (red and blue traces) of $UO_5H_2^-$ obtained under the same experimental conditions using the approach described in the text. The observed peak at 860 cm^{-1} is in accord with the single peak computed for the lower-energy $UO_3(OH)_2^-$ chemisorption (hydrolysis) structure, and not with the $UO_4(H_2O)^-$ physisorption (hydrate) structure.

DOI: 10.1021/acs.inorgchem.7b00144
Inorg. Chem. 2017, 56, 3686−3694

range of 650−1000 cm^{-1} (Figure 7) shows a single intense peak at 860 cm^{-1}. The single observed peak can be assigned to the uranyl asymmetric stretch frequency predicted from calculations to be at 938 cm^{-1} with PBE0 and 896 cm^{-1} with the B3LYP functional (both unscaled) for the hydroxide structure, $UO_3(OH)_2^-$. While the calculated frequency for the hydroxide structure is too high, it is well-known that with the chosen PBE0 or B3LYP functional frequencies are overestimated and need to be scaled to lower values.[56] Energetically, the hydroxide structure is predicted to be 114 kJ/mol lower in energy than the hydrate (Table 1). In addition, the computed spectrum for the alternative hydrate structure has two intense absorption features split by about 50 cm^{-1}, instead of the single peak observed in the experiment (see Figure S5). Both the difference in spectral features and relative energetics lead to the assignment of the 860 cm^{-1} peak to $UO_3(OH)_2^-$ rather than $UO_4(H_2O)^-$.

CONCLUSIONS

The two gas-phase pentavalent actinyl-oxalate anion complexes, $UO_2(C_2O_4)^-$ and $PaO_2(C_2O_4)^-$, were prepared by different routes. The uranium complex resulted from ESI and/or fragmentation during transfer to the ion trap. In contrast, the protactinium complex was not apparent upon ESI/transfer but was instead produced by CID of $Pa(C_2O_4)_3^-$ in the ion trap. It is feasible that $UO_2(C_2O_4)^-$ was not generated by ESI, but rather in the gas phase by fragmentation of $UO(C_2O_4)_2^-$ or $U(C_2O_4)_3^-$, which may be more susceptible to fragmentation than $Pa(C_2O_3)_3^-$.

The $UO_2(C_2O_4)^-$ complex spontaneously reacts with O_2 to yield UO_4^-, a process enabled by the creation of two CO_2 molecules. The computed structure of UO_4^- is doublet C_{2v} with a U $5f^0$ configuration; the structure is essentially a distorted $U^{VI}O_c^{2+}$ complex with two U−O_{yl} oxygen bonds and two equivalent U−O_{eq} bonds with a bond order intermediated between one and two. Formation UO_4^- from $UO_2(C_2O_4)^-$ proceeds via addition of O_2 to yield the superoxide complex $U^{VI}O_2(C_2O_4)(O_2)^-$. The $PaO_2(C_2O_4)^-$ complex does not exhibit similar reactivity, which can be traced to the resistance for oxidation from Pa^V to Pa^{VI}, resulting in endothermic addition of O_2 to yield $PaO_2(C_2O_4)(O_2)^-$. The disparate reactivities of $UO_2(C_2O_4)^-$ and $PaO_2(C_2O_4)^-$ with O_2 are well-predicted by the computed reaction energies.

The IRMPD spectrum of the isolated $UO_5H_2^-$ species in the uranyl asymmetric stretch region was measured. Calculated structures, energetics and IR spectra show that the species is that of a hydroxide, $UO_3(OH)_2^-$, rather than the hydrate, $UO_4(H_2O)^-$.

The novel oxidation reaction of $U^VO_2(C_2O_4)^-$ to yield $U^{VI}O_4^-$ suggests this as a potential route to oxidation of the transuranium actinides, An = Np, Pu, and Am. In contrast to U, for the subsequent actinides oxidation states above VI are feasible and may be accessible by replacement of C_2O_4 in $AnO_2(C_2O_4)^-$ by O_2 to yield AnO_4^-.

ASSOCIATED CONTENT

Supporting Information

The Supporting Information is available free of charge on the ACS Publications website at DOI: 10.1021/acs.inorgchem.7b00144.

ESI mass spectrum of protactinium and uranium oxalate solutions, CID of protactinium oxalate anion complexes, results for addition of water to $PaO(C_2O_4)_2^-$ and $PaO_2(C_2O_4)^-$, gas-phase reaction of $U^{16}O_4^-$ with $H_2{}^{18}O$, and complete computational results for all protactinium and uranium species considered (PDF)

AUTHOR INFORMATION

Corresponding Authors

*E-mail: wadejong@lbl.gov.
*E-mail: jkgibson@lbl.gov.

ORCID

Wibe A. de Jong: 0000-0002-7114-8315
Joaquim Marçalo: 0000-0001-7580-057X
Theodore A. Corcovilos: 0000-0001-5716-1188
Jonathan Martens: 0000-0001-9537-4117
John K. Gibson: 0000-0003-2107-5418

Notes

The authors declare no competing financial interest.

ACKNOWLEDGMENTS

This work was supported by the U.S. Department of Energy, Office of Basic Energy Sciences, Heavy Element Chemistry, at LBNL under Contract No. DE-AC02-05CH11231 [P.D.D. and J.K.G], by the U.S. Department of Energy Basic Energy Sciences, Early Career Research Award Program, under Contract DE-AC02-06CH11357 [R.E.W.], by the Fundação para a Ciência e a Tecnologia through RNEM-Portuguese Mass Spectrometry Network and project UID/Multi/04349/2013 [J.M.], by start-up funds from the Bayer School of Natural and Environmental Sciences and Duquesne University [M.V.S. and T.A.C.], and by The Netherlands Organisation for Scientific Research (NWO) under vici-grant no. 724.011.002 and the Stichting Physica [J.O.]. This research used resources of the National Energy Research Scientific Computing Center (NERSC), which is supported by the Office of Science of the U.S. Department of Energy under Contract No. DE-AC02-05CH11231. Some of the calculations were performed using the Oak Ridge Leadership Computing Facility, which is a DOE Office of Science User Facility supported under Contract DE-AC05-00OR22725. An award of computer time was provided by the Innovative and Novel Computational Impact on Theory and Experiment (INCITE) program. The authors are grateful to Professor Lester Andrews of the University of Virginia for providing the $^{18}O_2$ used in this work.

REFERENCES

(1) Schwarz, H. Relativistic effects in gas-phase ion chemistry: An experimentalist's view. *Angew. Chem., Int. Ed.* **2003**, *42*, 4442−4454.
(2) O'Hair, R. A. J. The 3D quadrupole ion trap mass spectrometer as a complete chemical laboratory for fundamental gas-phase studies of metal mediated chemistry. *Chem. Commun.* **2006**, 1469−1481.
(3) O'Hair, R. A. J.; Rijs, N. J. Gas Phase Studies of the Pesci Decarboxylation Reaction: Synthesis, Structure, and Unimolecular and Bimolecular Reactivity of Organometallic Ions. *Acc. Chem. Res.* **2015**, *48*, 329−340.
(4) Zhou, S. D.; Li, J. L.; Schlangen, M.; Schwarz, H. Bond Activation by Metal-Carbene Complexes in the Gas Phase. *Acc. Chem. Res.* **2016**, *49*, 494−502.
(5) Rodgers, M. T.; Armentrout, P. B. Cationic Noncovalent Interactions: Energetics and Periodic Trends. *Chem. Rev.* **2016**, *116*, 5642−5687.
(6) O'Hair, R. A. J. Mass spectrometry based studies of gas phase metal catalyzed reactions. *Int. J. Mass Spectrom.* **2015**, *377*, 121−129.

DOI: 10.1021/acs.inorgchem.7b00144
Inorg. Chem. 2017, 56, 3686−3694

(7) Plattner, D. A. Electrospray mass spectrometry beyond analytical chemistry: studies of organometallic catalysis in the gas phase. *Int. J. Mass Spectrom.* **2001**, *207*, 125−144.
(8) Bohme, D. K.; Schwarz, H. Gas-phase catalysis by atomic and cluster metal ions: The ultimate single-site catalysts. *Angew. Chem., Int. Ed.* **2005**, *44*, 2336−2354.
(9) Operti, L.; Rabezzana, R. Gas-phase ion chemistry in organometallic systems. *Mass Spectrom. Rev.* **2006**, *25*, 483−513.
(10) Chen, P. Electrospray ionization tandem mass spectrometry in high-throughput screening of homogeneous catalysts. *Angew. Chem., Int. Ed.* **2003**, *42*, 2832−2847.
(11) Schreckenbach, G.; Shamov, G. A. Theoretical Actinide Molecular Science. *Acc. Chem. Res.* **2010**, *43*, 19−29.
(12) Groenewold, G. S.; Gianotto, A. K.; Cossel, K. C.; Van Stipdonk, M. J.; Moore, D. T.; Polfer, N.; Oomens, J.; de Jong, W. A.; Visscher, L. Vibrational spectroscopy of mass-selected [UO2(ligand)-(n)](2+) complexes in the gas phase: Comparison with theory. *J. Am. Chem. Soc.* **2006**, *128*, 4802−4813.
(13) Groenewold, G. S.; Van Stipdonk, M.; Gresham, G. L.; Oomens, J.; de Jong, B.; Gianotto, A. K.; McIlwain, M. E. Combined infrared and computational studies of discrete uranyl trianion complexes. *Abstr Pap Am. Chem. Soc.* **2007**, 234.
(14) Groenewold, G. S.; Gianotto, A. K.; McIlwain, M. E.; Van Stipdonk, M. J.; Kullman, M.; Moore, D. T.; Polfer, N.; Oomens, J.; Infante, I.; Visscher, L.; Siboulet, B.; De Jong, W. A. Infrared spectroscopy of discrete uranyl anion complexes. *J. Phys. Chem. A* **2008**, *112*, 508−521.
(15) Groenewold, G. S.; de Jong, W. A.; Oomens, J.; Van Stipdonk, M. J. Variable Denticity in Carboxylate Binding to the Uranyl Coordination Complexes. *J. Am. Soc. Mass Spectrom.* **2010**, *21*, 719−727.
(16) Groenewold, G. S.; van Stipdonk, M. J.; Oomens, J.; de Jong, W. A.; Gresham, G. L.; McIlwain, M. E. Vibrational spectra of discrete UO22+ halide complexes in the gas phase. *Int. J. Mass Spectrom.* **2010**, *297*, 67−75.
(17) Michelini, M. D.; Marçalo, J.; Russo, N.; Gibson, J. K. Gas-Phase Reactions of Uranate Ions, UO2-, UO3-, UO4-, and UO4H-, with Methanol: a Convergence of Experiment and Theory. *Inorg. Chem.* **2010**, *49*, 3836−3850.
(18) Czekner, J.; Lopez, G. V.; Wang, L. S. High resolution photoelectron imaging of UO- and UO2- and the low-lying electronic states and vibrational frequencies of UO and UO2. *J. Chem. Phys.* **2014**, *141*, 244302.
(19) Hunt, R. D.; Andrews, L. Reactions of Pulsed-Laser Evaporated Uranium Atoms with Molecular-Oxygen - Infrared-Spectra of UO, UO2, UO3, UO2+, UO22+, and UO3-O2 in Solid Argon. *J. Chem. Phys.* **1993**, *98*, 3690−3696.
(20) Kushto, G. P.; Souter, P. F.; Andrews, L.; Neurock, M. A matrix isolation FT-IR and quasirelativistic density functional theory investigation of the reaction products of laser-ablated uranium atoms with NO, NO2 and N2O. *J. Chem. Phys.* **1997**, *106*, 5894−5903.
(21) Wang, X. F.; Andrews, L.; Li, J.; Bursten, B. E. Significant interactions between uranium and noble-gas atoms: Coordination of the UO2+ cation by Ne, Ar, Kr, and Xe atoms. *Angew. Chem., Int. Ed.* **2004**, *43*, 2554−2557.
(22) Jin, J.; Lue, C. J.; Heaven, M. C. Matrix isolation spectroscopy of uranium oxides. *Abstr Pap Am. Chem. Soc.* **2006**, 231.
(23) Heaven, M. C.; Goncharov, V.; Steimle, T. C.; Ma, T. M.; Linton, C. The permanent electric dipole moments and magnetic g factors of uranium monoxide. *J. Chem. Phys.* **2006**, *125*, 204314.
(24) Kovacs, A.; Konings, R. J. M.; Gibson, J. K.; Infante, I.; Gagliardi, L. Quantum Chemical Calculations and Experimental Investigations of Molecular Actinide Oxides. *Chem. Rev.* **2015**, *115*, 1725−1759.
(25) Bodo, E.; Ciavardini, A.; Dalla Cort, A.; Giannicchi, I.; Yafteh Mihan, F.; Fornarini, S.; Vasile, S.; Scuderi, D.; Piccirillo, S. Anion Recognition by Uranyl-Salophen Derivatives as Probed by Infrared Multiple Photon Dissociation Spectroscopy and Ab Initio Modeling. *Chem. - Eur. J.* **2014**, *20*, 11783−11792.
(26) Bryantsev, V. S.; de Jong, W. A.; Cossel, K. C.; Diallo, M. S.; Goddard, W. A.; Groenewold, G. S.; Chien, W.; Van Stipdonk, M. J. Two-electron three-centered bond in side-on (eta(2)) uranyl(V) superoxo complexes. *J. Phys. Chem. A* **2008**, *112*, 5777−5780.
(27) Ricks, A. M.; Gagliardi, L.; Duncan, M. A. Uranium Oxo and Superoxo Cations Revealed Using Infrared Spectroscopy in the Gas Phase. *J. Phys. Chem. Lett.* **2011**, *2*, 1662−1666.
(28) Keller, C. Chemistry of Protactinium. *Angew. Chem., Int. Ed. Engl.* **1966**, *5*, 23−35.
(29) Altmaier, M.; Gaona, X.; Fanghanel, T. Recent Advances in Aqueous Actinide Chemistry and Thermodynamics. *Chem. Rev.* **2013**, *113*, 901−943.
(30) Le Naour, C.; Trubert, D.; Di Giandomenico, M. V.; Fillaux, C.; Den Auwer, C.; Moisy, P.; Hennig, C. First structural characterization of a protactinium(V) single oxo bond in aqueous media. *Inorg. Chem.* **2005**, *44*, 9542−9546.
(31) Dau, P. D.; Wilson, R. E.; Gibson, J. K. Elucidating Protactinium Hydrolysis: The Relative Stabilities of PaO2(H2O)(+) and PaO(OH)(2)(+). *Inorg. Chem.* **2015**, *54*, 7474−7480.
(32) Sokalska, M.; Prussakowska, M.; Hoffmann, M.; Gierczyk, B.; Franski, R. Unusual Ion UO4- Formed Upon Collision Induced Dissociation of [UO2(NO3)(3)](−), [UO2(ClO4)(3)](−), [UO2-(CH3COO)(3)](−) Ions. *J. Am. Soc. Mass Spectrom.* **2010**, *21*, 1789−1794.
(33) Gong, Y.; Gibson, J. K. Formation and Characterization of the Uranyl-SO2 Complex, UO2(CH3SO2) (SO2)(−). *J. Phys. Chem. A* **2013**, *117*, 783−787.
(34) Rios, D.; Rutkowski, P. X.; Shuh, D. K.; Bray, T. H.; Gibson, J. K.; Van Stipdonk, M. J. Electron transfer dissociation of dipositive uranyl and plutonyl coordination complexes. *J. Mass Spectrom.* **2011**, *46*, 1247−1254.
(35) Gronert, S. Estimation of effective ion temperatures in a quadrupole ion trap. *J. Am. Soc. Mass Spectrom.* **1998**, *9*, 845−848.
(36) Rios, D.; Michelini, M. C.; Lucena, A. F.; Marçalo, J.; Bray, T. H.; Gibson, J. K. Gas-Phase Uranyl, Neptunyl, and Plutonyl: Hydration and Oxidation Studied by Experiment and Theory. *Inorg. Chem.* **2012**, *51*, 6603−6614.
(37) Lucena, A. F.; Carretas, J. M.; Marçalo, J.; Michelini, M. C.; Gong, Y.; Gibson, J. K. Gas-Phase Reactions of Molecular Oxygen with Uranyl(V) Anionic Complexes-Synthesis and Characterization of New Superoxides of Uranyl(VI). *J. Phys. Chem. A* **2015**, *119*, 3628−3635.
(38) Oepts, D.; van der Meer, A. F. G.; van Amersfoort, P. W. The free-electron Laser user facility FELIX. *Infrared Phys. Technol.* **1995**, *36*, 297−308.
(39) Hu, S. X.; Gibson, J. K.; Li, W. L.; Van Stipdonk, M. J.; Martens, J.; Berden, G.; Redlich, B.; Oomens, J.; Li, J. Electronic structure and characterization of a uranyl di-15-crown-5 complex with an unprecedented sandwich structure. *Chem. Commun.* **2016**, *52*, 12761−12764.
(40) Dau, P. D.; Rios, D.; Gong, Y.; Michelini, M. C.; Marçalo, J.; Shuh, D. K.; Mogannam, M.; Van Stipdonk, M. J.; Corcovilos, T. A.; Martens, J. K.; Oomens, J.; Berden, G.; Redlich, B.; Gibson, J. K. Synthesis and hydrolysis of uranyl, neptunyl and plutonyl gas-phase complexes exhibiting discrete actinide-carbon bonds. *Organometallics* **2016**, *35*, 1228−1240.
(41) Martens, J.; Berden, G.; Gebhardt, C. R.; Oomens, J. Infrared Ion Spectroscopy in a Modified Quadrupole Ion Trap Mass Spectrometer at the FELIX Free Electron Laser Laboratory. *Rev. Sci. Instrum.* **2016**, *87*, 103108.
(42) Martens, J.; Grzetic, J.; Berden, G.; Oomens, J. Structural identification of electron transfer dissociation products in mass spectrometry using infrared ion spectroscopy. *Nat. Commun.* **2016**, *7*, 11754.
(43) Valiev, M.; Bylaska, E. J.; Govind, N.; Kowalski, K.; Straatsma, T. P.; Van Dam, H. J. J.; Wang, D.; Nieplocha, J.; Apra, E.; Windus, T. L.; de Jong, W. NWChem: A comprehensive and scalable open-source solution for large scale molecular simulations. *Comput. Phys. Commun.* **2010**, *181*, 1477−1489.

DOI: 10.1021/acs.inorgchem.7b00144
Inorg. Chem. 2017, 56, 3686−3694

(44) Adamo, C.; Barone, V. Toward reliable density functional methods without adjustable parameters: The PBE0 model. *J. Chem. Phys.* **1999**, *110*, 6158−6170.
(45) Kuchle, W.; Dolg, M.; Stoll, H.; Preuss, H. Energy-Adjusted Pseudopotentials for the Actinides - Parameter Sets and Test Calculations for Thorium and Thorium Monoxide. *J. Chem. Phys.* **1994**, *100*, 7535−7542.
(46) Godbout, N.; Salahub, D. R.; Andzelm, J.; Wimmer, E. Optimization of Gaussian-Type Basis-Sets for Local Spin-Density Functional Calculations 0.1. Boron through Neon, Optimization Technique and Validation. *Can. J. Chem.* **1992**, *70*, 560−571.
(47) Maurice, R.; Renault, E.; Gong, Y.; Rutkowski, P. X.; Gibson, J. K. Synthesis and Structures of Plutonyl Nitrate Complexes: Is Plutonium Heptavalent in PuO3(NO3)(2)(−) ? *Inorg. Chem.* **2015**, *54*, 2367−2373.
(48) Keith, T. A. *AIMAll*, 17.01.25 ed.; TK Gristmill Software: Overland Park KS, USA, 2017.
(49) Vasiliu, M.; Peterson, K. A.; Gibson, J. K.; Dixon, D. A. Reliable Potential Energy Surfaces for the Reactions of H2O with ThO2, PaO2+, UO22+, and UO2+. *J. Phys. Chem. A* **2015**, *119*, 11422−11431.
(50) Kaltsoyannis, N. Covalency hinders AnO(2)(H2O)(+) -> AnO(OH)(2)(+) isomerisation (An = Pa-Pu). *Dalton T* **2016**, *45*, 3158−3162.
(51) Siboulet, B.; Marsden, C. J.; Vitorge, P. What can quantum chemistry tell us about Pa(v) hydration and hydrolysis? *New J. Chem.* **2008**, *32*, 2080−2094.
(52) Spezia, R.; Siboulet, B.; Abadie, S.; Vuilleumier, R.; Vitorge, P. Stability and Instability of the Isoelectronic UO22+ and PaO2+ Actinyl Oxo-Cations in Aqueous Solution from Density Functional Theory Based Molecular Dynamics. *J. Phys. Chem. B* **2011**, *115*, 3560−3570.
(53) Toraishi, T.; Tsuneda, T.; Tanaka, S. Theoretical study on molecular property of protactinium(V) and uranium(VI) oxocations: Why does protactinium(V) form monooxo cations in aqueous solution? *J. Phys. Chem. A* **2006**, *110*, 13303−13309.
(54) Su, J.; Li, W. L.; Lopez, G. V.; Jian, T.; Cao, G. J.; Li, W. L.; Schwarz, W. H. E.; Wang, L. S.; Li, J. Probing the Electronic Structure and Chemical Bonding of Mono-Uranium Oxides with Different Oxidation States: UOx- and UOx (x = 3−5). *J. Phys. Chem. A* **2016**, *120*, 1084−1096.
(55) Schroder, D.; Souvi, S. O.; Alikhani, E. Hydrated metal-oxide versus dihydroxide structures of [MO2H2](+) cations with M = Fe, Co, and Ni. *Chem. Phys. Lett.* **2009**, *470*, 162−165.
(56) Kesharwani, M. K.; Brauer, B.; Martin, J. M. L. Frequency and Zero-Point Vibrational Energy Scale Factors for Double-Hybrid Density Functionals (and Other Selected Methods): Can Anharmonic Force Fields Be Avoided? *J. Phys. Chem. A* **2015**, *119*, 1701−1714.

DOI: 10.1021/acs.inorgchem.7b00144
Inorg. Chem. 2017, 56, 3686−3694